Available online at www.sciencedirect.com
SCIENCE DIRECT®
International Journal of Engineering Science 43 (2005) 1486–1497
International Journal of Engineering Science
www.elsevier.com/locate/ijengsci

Dusty debris in tornadoes modelled by high Reynolds number two cells vortices

Arnaud Chauvière, Joël Chaskalovic *

Laboratoire de Modélisation en Mécanique, CNRS and Université Pierre et Marie Curie (Paris VI), 8 rue du Capitaine Scott, 75015 Paris, France

Received 16 September 2004; received in revised form 8 August 2005; accepted 8 August 2005

Abstract

Exact solutions of Navier–Stokes equations enable to describe nice features of atmospherical flows as tornadoes. For this very particular and singular kind of fluid motions, the flows are very often modelled by conical solutions. Famous authors as Burgers (1948) [J.M. Burgers, A mathematical model illustrating the theory of turbulence, Advan. Appl. Mech. 1 (1948) 197–199], Rott (1958) [N. Rott, On the viscous core of a line vortex, Z. Angew. Math. Phys. 96 (1958) 543–553], Serrin (1972) [J. Serrin, The swirling vortex, Phil. Trans. Roy. Soc. Lond. A 271 (1972) 320–360; J. Serrin, The swirling vortex, Phil. Trans. Roy. Soc. Lond. A 271 (1972) 357–358] and Goldshtik and Shtern (1990) [M. Goldshtik, V. Shtern, J. Fluid Mech. 218 (1990) 483–508], improved greatly research. Most of the time, except Serrin's model, these models applied to tornadoes, rather produced fields of velocity, with orders of magnitudes which are way too low to be appropriate for describing thunderstorms observed in meteorology. Moreover, these models do not include any explicit mechanisms which take into account the potential actions of dust particles often present in tornadoes. Here, we do suggest a new way of modelling the mature phase of a tornado by considering two swirling cells separated by a intermediate cone, which position results by the equilibrium of normal stresses exerted on the two sides of the cone. This choice of modelling is motivated by considering two kinds of flows, inside and outside the cone, to get significant and different characteristics of the associated resulting vortices. This equilibrium condition, completed by the discontinuity of the tangential stresses on the cone, leads to realistic magnitude of the velocity field, i.e., about 10^2 m s^{-1}. This discontinuity is motivated by several observations which show the ejection of dust particles along a specific cone direction. At our modelling scale, we do want to model the integral of the dragging forces, resulting from the motion of those particles inside the fluid, by a discontinuity of the tangential stresses on the cone which split the flows into two separate cells.

1. Introduction

The observation, the modelling and the understanding of atmospherical tornadoes have experienced over the last twelve years many new developments. But, despite numerous tools—especially those connected with

* Corresponding author. Tel.: +33 1 44 27 26 91; fax: +33 1 44 27 52 59.
E-mail addresses: chauvier@lmm.jussieu.fr (A. Chauvière), jch@moka.ccr.jussieu.fr (J. Chaskalovic).

0020-7225/$ - see front matter
doi:10.1016/j.ijengsci.2005.08.001

numerical simulations—it is interesting to develop models based on exact solutions of Navier–Stokes equations because they are useful in determining singular conditions, under which these vortices could emerge [1].

Moreover, the discovery of new exact solutions of Navier–Stokes equations also enabled us to evaluate geometric features of the flows, and more globally, the relation between different mechanisms which are included in the model and the shape of streamlines, obtained by simulations of the resulting flows.

Unfortunately, the class of exact solutions of Navier–Stokes equations modelling tornadoes which matches realistic features—streamlines geometry or tornadoes phenomenology—[2,4], often leads to very small numerical orders of magnitude of velocity fields, except Serrin's model.

Moreover, when the modelling process leads to describe a two cells rotating flow, along the cone which separates the two cells, boundary conditions are not appropriate to model the observations.

More precisely, Serrin [3] motivated the existence of an intermediate cone inside a two cells flow by the presence of dust particles ejected along the cone which are observed for a large class of tornadoes.

The resulting flow he got is certainly a pioneering contribution to describe, in a certain way, the presence of dust debris inside a swirling vortex.

But, the explicit contribution of the particles actions on the fluid is not taken into account in his approach, particularly, the drag forces which are contact forces on the fluid.

It's the reason why we propose to complete Serrin's model by explicitly considering these external forces in our model. As a consequence, one must take into account along the cone a tangential discontinuity boundary condition.

Our target is to get a mathematical model which is in line with physical observations [5] and which match with real tornadoes.

To illustrate our purpose, let's consider in detail Serrin's model [2] which is sufficiently representative in connection with the assumptions which are assumed in usual conical flows modelling: his construction describes three kinds of flows satisfying the adherence condition on the ground. Existence of flows depend on the following driving parameters: the vertical shear near the ground τ_r and the rate of the azimuthal rotation Γ.

So, when the shear τ_r is positive, the fluid is ejected outward along the ground. When it is negative, the fluid moves toward the central axis of the vortex. In this last case, two kinds of flows can emerge. They depend on the density sign of the shear $\mathscr{T}$ near the central axis: the flow is either an updraft ($\mathscr{T} > 0$) or, when the fluid is descending along the central axis ($\mathscr{T} < 0$), an intermediate jet appears inside the flow, for compatibility between the descending flow, near the central axis and the inward flow, near the ground.

Moreover, laboratory experiments [6] and numerical simulations [7] also underlined the interest for this last kind of flows constituted by two cells.

In addition, Serrin [3] remarked the particular interest of these flows because the intermediate cone may explain physical observations describing dust debris particles that are moving and ejected in a specific direction inside the flow, and precisely modelled by the cone separation between the two cells [2].

Because the action of those numerous debris on the fluid is not taken into account in the classical process of modelling conical flows, we propose a new family of exact and axisymmetric solutions of the steady and incompressible Navier–Stokes equations. These solutions are in agreement with the existence of this matter inside the fluid, particularly dusty debris, which exerted on the fluid contact forces.

To this end, first we will consider two conical flows separated by a given fictive cone for an arbitrary angle. This global position of our modelling is different from Serrin's: his stance is to consider a unique conical flow on half a space above a given plane.

Secondly, on each side of the arbitrary cone we introduced, we will consider a conical flow inside and outside the cone (see Fig. 1(a)). Each of these conical flows will be defined as a solution which has the same mathematical structure that a given solution of Serrin's model.

More precisely, the inner flow we choose describes a fast swirling and descending flow inside a given cone, which satisfies a slip condition on the border of the cone. On the other hand, the flow outside the cone is taken as a slow and swirling updraft, sliding on the cone, which corresponds to a Serrin's solution in a slightly different geometry (see Fig. 1(b)).

Finally, on the cone separation, we will introduce the discontinuity of the tangential stresses to take into account the presence of dusty debris at this neighborhood of the cone frontier, and then, to model their actions on the fluid.

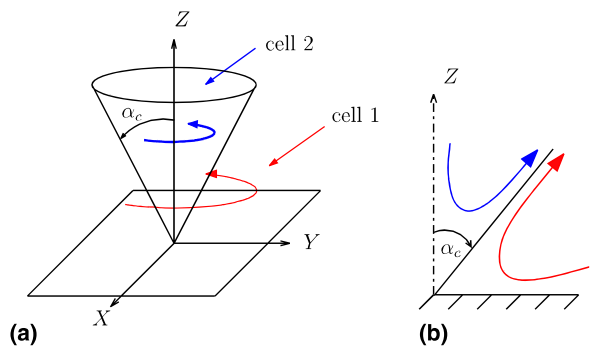

Fig. 1. Two cells flow configuration: (a) 3D-visualisation; (b) meridian plane.

2. Mathematical modelling

2.1. Flow configuration

We introduce the spherical polar coordinates (O; R, α, θ), where R denotes the radial distance from the origin, α is the angle between the radius vector and the positive Z-axis, and θ is the meridian angle about the Z-axis. The positive Z-axis is then described by $\alpha = 0$ is the central axis of the vortex, the boundary plane $Z = 0$ by $\alpha = \pi/2$ models the tangent plane with the earth. The respective physical components of the velocity vector $\vec{V}$ in this coordinate system will be denoted u, v and w.

Then, our modelling consists of two cells, separated by a fictive cone defined by α_c, each one possessing its own level of azimuthal rotation. The cell 1 is defined by $x \in [0, x_c]$ and the cell 2 by $x \in [x_c, 1[$, where $x = \cos\alpha$ and $x_c = \cos\alpha_g c$. In each cell, the spherical components of the field of velocity are determined by

$$u_i(x,R) = \frac{\Gamma_i F_i'(x)}{R}, \quad v_i(x,R) = \frac{\Gamma_i F_i(x)}{R\sqrt{1-x^2}}, \quad w_i(x,R) = \frac{\Gamma_i \Omega_i(x)}{R\sqrt{1-x^2}} \tag{1}$$

for $i \in \{1, 2\}$, where the functions F_i and Ω_i are the no-dimensioned unknown functions and the circulation Γ_i defines a swirling Reynolds number $\mathscr{R}_{e_i} = \Gamma_i/v$ corresponding to each cell.

2.2. Interface modelling and boundary conditions

The separation surface ($\alpha = \alpha_c$) between the two cells is modelled as an interface defined by an impermeable cone on which we assure the continuity of the fields of velocity and pressure. This last condition will determine the position of the cone $\alpha = \alpha_c$. In other words, this angle is then obtained by the equilibrium condition corresponding to the compensation between normal stresses.

So, on the interface $x = x_c$, the conditions of continuity will be written as follows:

$$F_2'(x_c) = \chi F_1'(x_c), \quad F_2(x_c) = F_1(x_c) = 0 \quad \text{and} \quad \Omega_2(x_c) = \chi\Omega_1(x_c), \tag{2}$$

where χ is the ratio $\mathscr{R}_{e_1}/\mathscr{R}_{e_2}$. Moreover, $F_i'(x_c)$, where $i = 1, 2$, will be positive to guaranty that the fluid is ejected on each side and above the cone separation surface.

At this stage of our presentation, we notice that no condition was imposed on the continuity of the tangential stresses on the cone. In fact, we do not want any continuity of these stresses because this would lead us to Serrin's model which does not describe the interaction between dusty debris—often moving inside tornadoes' flows—and the fluid.

More precisely, we do want to consider a discontinuity of the tangential stresses on the cone as the result of the existence of dragging forces developed by the matter in this region of the flow, moving outward the central axis of the vortex and along a specific cone direction.

In this way, the line of discontinuity $x = x_c$ represents, on a large scale description, the action of the dust and the debris on the fluid in a privileged direction; the one that Serrin highlighted in his paper, when he considered a conical flow made of a double cells.

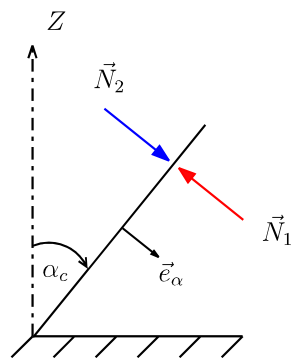

Fig. 2. Equilibrium of the cone in a meridian plane: compensation of normal efforts $\vec{N}_1$ and $\vec{N}_2$.

This is the main and important difference between our choice of modelling the junction between the two cells flow, in comparison with Serrin's model. Moreover, in his model, the line position ($\alpha = \alpha_c$) is determined by the driving flows parameters. In our, the cone frontier position is determined by the equilibrium of the normal component of the stresses $\vec{N}_i$, where $i = 1, 2$, resulting from the pressure on the two sides of the cone. Thus, the equilibrium angle α_c is given by the relation $\vec{N}_1 + \vec{N}_2 = \vec{0}$ (see Fig. 2).

Concerning the other boundary conditions used by Serrin, namely, the adherence condition on ground (i.e., $Z = 0$), the behavior of a free vortex near the central axis and also the impossibility that the flow presents a central line which develops either a source or a sink, they will be maintained in our model. This leads to the following boundary conditions [2]:

$$F_1 = F_1' = \Omega_1 = 0 \quad \text{at} \quad x = 0, \qquad F_2 = 0 \quad \text{and} \quad \Omega_2 = 1 \quad \text{when } x \text{ goes to } 1.$$

2.3. Mathematical formulation

The model we described in the last section leads us [8] to the following mathematical problem ($\mathscr{P}$) in which, for each cell, the flow is determined by the couple of parameters $(q_i, \mathscr{R}_{e_i})$, $(i = 1,2)$, where q_i is characteristic of the intensity of the shear inside each cell. The resulting mathematical formulation ($\mathscr{P}$) is as follows:

$$(\mathscr{P})\begin{cases} (\mathscr{P}_1)\begin{cases} \frac{1}{\mathscr{R}_{e_1}}\left[2(1-x^2)F_1' + 4xF_1\right] + F_1^2 = H_1(x), F_1(0) = 0, \\ \frac{1}{\mathscr{R}_{e_1}}(1-x^2)\Omega_1'' + F_1\Omega_1' = 0, \Omega_1(0) = 0, \Omega_1(x_c) = 1, \end{cases} & \forall x \in]0, x_c[, \\ (\mathscr{P}_2)\begin{cases} \frac{1}{\mathscr{R}_{e_2}}\left[2(1-x^2)F_2' + 4xF_2\right] + F_2^2 = H_2(x), F_2(x_c) = 0, \\ \frac{1}{\mathscr{R}_{e_2}}(1-x^2)\Omega_2'' + F_2\Omega_2' = 0, \Omega_2(x_c) = \chi, \Omega_2(1) = 1, \end{cases} & \forall x \in]x_c, 1[, \end{cases}$$

where H_1 and H_2 are given by

$$H_1(x) = -q_1 x(x_c - x) + \frac{2F_1'(x_c)}{\mathscr{R}_{e_1}}(1 - x_c^2)\frac{x}{x_c} + 2\left[1 - \left(x_c + \frac{1}{x_c}\right)x + x^2\right]\int_0^x \frac{t\Omega_1^2}{(1-t^2)^2}\,\mathrm{d}t$$
$$+ 2\frac{x}{x_c}\int_x^{x_c} \frac{\Omega_1^2}{(1-t^2)^2}(x_c - t)(1 - x_c t)\,\mathrm{d}t,$$

and

$$H_2(x) = -\left[q_2 + \frac{\chi^2}{1 - x_c^2}\right](x - x_c)(1 - x) + \frac{2F_2'(x_c)}{\mathscr{R}_{e_2}}(1 + x_c)(1 - x)$$
$$+ 2(1-x)^2\int_{x_c}^x \frac{t\Omega_2^2}{(1-t^2)^2}\,\mathrm{d}t + 2\frac{x - x_c}{1 - x_c}\int_x^1 \frac{\Omega_2^2}{(1+t)^2}\,\mathrm{d}t - 2x_c\frac{1-x}{1-x_c}\int_{x_c}^x \frac{\Omega_2^2}{(1+t)^2}\,\mathrm{d}t,$$

bearing in mind that $F_2'(x_c) = \chi F_1'(x_c)$ through (2).

To complete this formulation, one must take into account the equilibrium equation determining the position of the cone frontier α_c

$$q_1 + 2\int_0^{x_c} \frac{t\Omega_1^2(t)}{(1-t^2)^2}\,\mathrm{d}t = \frac{q_2}{\chi^2} + \frac{1}{1-x_c^2}. \tag{3}$$

Remark. The formulation of problem ($\mathscr{P}$) conserves the original structure of Serrin's model [2] if one considers for each vortex flow (inside and outside the cone), his general formulation.

To this end, one would have to replace our function H_1 and H_2 by his function G and to substitute our game of boundary conditions by his ones, namely with a total continuity of stresses along the interface played by the given cone.

2.4. Physical properties of the flows

In this section, we would like to focus our attention on the physical properties of the flows resulting from our choice of modelling. Particularly, we will give special attention to the physical meaning of the different parameters playing the fundamental role of driving the flow in each cell.

To this end, let us observe the expression of the tangential stresses that must lead to a gap for modelling a discontinuity on the cone (see the previous section). Indeed, radial stresses $\tau^i_{R_c}$ and azimuthal stresses $\tau^i_{\theta_c}$ are given by

$$\tau^i_{R_c} = \frac{\rho\Gamma_i^2}{2R^2}\frac{H_i'(x_c)}{\sqrt{1-x_c^2}} \quad \text{and} \quad \tau^i_{\theta_c} = \frac{\rho\Gamma_i^2}{R^2}\frac{1}{\mathscr{R}_{e_i}}\left(\Omega_i'(x_c) + \frac{2x_c\Omega_i(x_c)}{1-x_c^2}\right). \tag{4}$$

These quantities will be computed on each side of the cone and the result will be different on each side. This would be particularly easy to prove in the case when we will exhibit the existence of a boundary layer near the cone frontier, to describe high Reynolds number vortex inside the cone (see Section 3).

This gap will be valid, no matter what the continuity of the velocity is, no matter what the continuity of normal stresses are. Moreover, one can observe that the parameters of the model directly influence the stresses intensity (4) near the cone.

As far as the evolution of the cone frontier position $\alpha = \alpha_c$ is concerned, we have chosen to take into account a specific solution which is defined by the following values: $q_1 = 0.649$, $\mathscr{R}_{e_1} = 8.255$, $q_2 = -0.866$ and $\mathscr{R}_{e_2} = 10$.

We have singled out these values in order to analyze the evolution of flow characteristics, from a starting point which has features which are near from those of Serrin's solutions, in the case of a two cells flow.

But, the main difference of our modelling scheme with Serrin's model, is that the flow can be fixed outside the cone in our model without fixing the features of the flow inside the cone. We are thus in a position to increase progressively $\mathscr{R}_{e_2}$, in order to achieve high Reynolds vortices inside the cone frontier. This objective is to obtain a sufficiently high scale of velocity which will be in line with physical observations [5].

We now observe the evolution of the cone position depending on the characteristics of the flow inside the cone—cell 2. Consequently, we keep fixed all parameters except $\mathscr{R}_{e_2}$ for first observations (see Fig. 3(a)). Then, we leave the second parameter q_2 take different values (see Fig. 3(b)).

Therefore, when $\mathscr{R}_{e_2}$ is increasing, we observed that the cone frontier is moving toward the vortex central axis. In this case, the depressurizing phenomena, caused by the rotation, gets more and more intense. This is the reason why the cone keeps on closing itself when the parameter $\mathscr{R}_{e_2}$ increases.

When q_2 decreases, it is the vertical flow that goes faster toward the ground. It also accelerates the central depressurizing phenomena.

All of the above results may be obtained if we take into consideration that the equilibrium condition can be rewritten as follows:

$$x_c = \left[1 - \left(q_1 - \frac{q_2}{\chi^2} + 2\int_0^{x_c} \frac{t\Omega_1^2(t)}{(1-t^2)^2}\,\mathrm{d}t\right)^{-1}\right]^{1/2}. \tag{5}$$

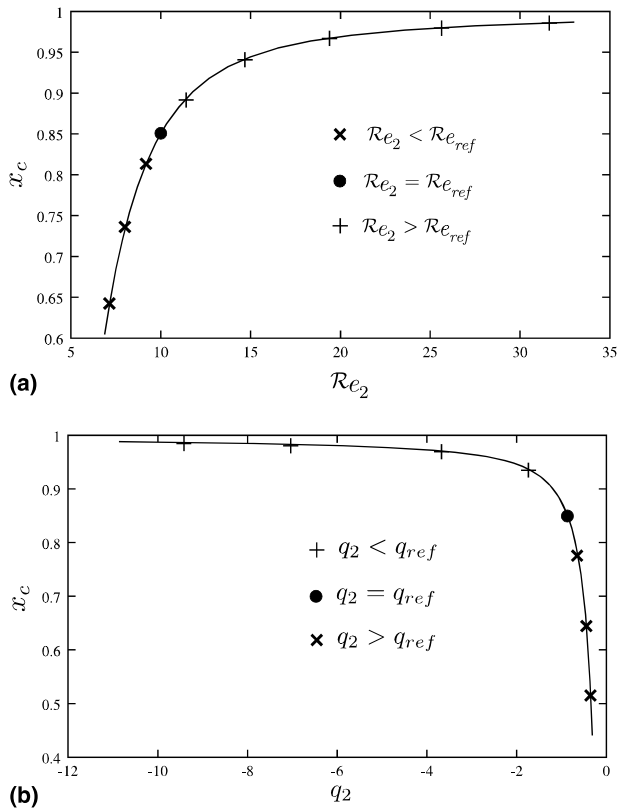

Fig. 3. Evolution of the cone position: values of parameters in cell 1 are fixed to $q_1 = 0.649$ and $\mathscr{R}_{e_1} = 8.255$. Specific values $q_2 = q_{\text{ref}} = -0.866$ and $\mathscr{R}_{e_2} = \mathscr{R}_{e_{\text{ref}}} = 10$ lead to Serrin's solutions. Variations of parameters in cell 2, from these reference values, show the evolution of the cone angle according to: (a) parameter $\mathscr{R}_{e_2}$ with $q_2 = q_{\text{ref}}$; (b) parameter q_2 with $\mathscr{R}_{e_2} = \mathscr{R}_{e_{\text{ref}}}$.

This formula demonstrates that the cone frontier depends both on the parameters q_1, $\mathscr{R}_{e_1}$ (through Ω_1), and on the ratio q_2/χ^2. Moreover, because the integral appearing in (5) may be upper bounded, it can be argued that the angle determination is only possible if the condition $q_2/\chi^2 \leqslant q_1 - 1$ is satisfied.

Then, we choose to represent the variations of the angle x_c as a function of $q_1 - q_2/\chi^2 - 1$, leading to an interval of variations, with a lower bound which is equal to zero (see Fig. 4(a) and (b)).

This analysis provides us with a physical interpretation of the two cells influence. More precisely, we now can interpret transitions between the three cases of flows in Serrin's model [2], as the cone frontier position we developed in our model.

Finally, contrary to the model of Shtern and Hussain [9], we will demonstrate in the following section that we will be able to build a model of high Reynolds number vortices without fixing arbitrarily the angle of the interface α_c. Therefore, in our model, the position of the cone frontier will be determined by the intensity of the velocity in each part of the flow, inside and outside the cone. In addition, the resulting flow will include new features concerning the influence of dusty debris inside the flow which exert contact forces on the fluid.

3. Swirling vortex at high Reynolds number

This section is devoted to high Reynolds number swirling vortex flows. Several authors as Fernandez et al. [10], Shtern and Hussain [11], treat these kinds of swirling conical vortices. But, here, our aim is to develop a model that allows a difference in the velocities amplitude—inside and outside the cone frontier—in agreement with a discontinuity of stresses on the cone frontier between the two cells. This feature is the main difference with the works we mentioned before.

To this end, we will consider high values of the Reynolds number $\mathscr{R}_{e_2}$ which describes rotation characteristics inside the cone.

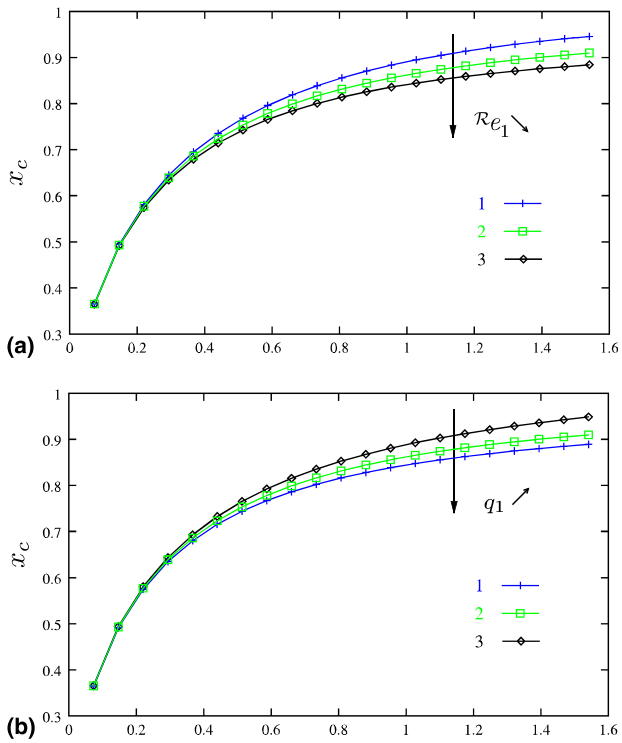

Fig. 4. Evolution of the cone position as a function of the composed variable $q_1 - q_2/\chi^2 - 1$: (a) with $\mathscr{R}_{e_1} = 11$ (1), 8.2545 (2), 2 (3); (b) with $q_1 = 0.949$ (1), 0.649 (2), 0.349 (3).

As already demonstrated in the previous section, when the other parameters remain fixed, the cone frontier gradually closes due to the intensification of the vertical and azimuthal velocities near the central axis. After fixing parameters values $(q_1, \mathscr{R}_{e_1})$, we will increase $\mathscr{R}_{e_2}$ while adjusting the value of the parameter q_2 in order to have q_2/χ^2 constant. As a result, the value of the angle α_c will be determined through formula (3).

Moreover, the flow in the cell 1, near the ground, is entirely determined in a way that it is structured with one branch only, ascending on the cone frontier. In top of that, we will choose negative value of the parameter q_2 so that the flow inside the cone is also structured with one branch only, descending along the central axis [8].

By numerical simulations of problem $(\mathscr{P}_2)$ solutions, we have noticed (see Fig. 5) that solutions (F_2, Ω_2) tend to reach a limit corresponding to a vortical inviscid flow. These observations have led us to develop an asymptotic analysis inside the cone.

Bearing in mind this remark, we consider $\mathscr{R}_{e_1} = \mathscr{O}(1)$ as well as we introduce the small parameter $\epsilon = 1/\mathscr{R}_{e_2}$ with $\mathscr{R}_{e_2} \gg 1$. The boundary surface $x = x_c$ is fixed by the constant value of q_2/χ^2 and because we have $\chi = \epsilon\mathscr{R}_{e_1} \ll 1$, then $q_2 = \mathscr{O}(\epsilon^2\mathscr{R}_{e_1}^2) \ll 1$.

Taking into account these parameters amplitudes, we are now able to develop the asymptotic analysis of problem $(\mathscr{P}_2)$ solutions. The first order of the outer solution is then given by

$$\begin{aligned} F_2(x,\epsilon) &= F_0(x) = \sqrt{\frac{(1-x)(x-x_c)}{1-x_c^2}}, \\ \Omega_2(x,\epsilon) &= \Omega_0(x) = 1. \end{aligned} \tag{6}$$

We introduce the inner variable

$$\tilde{x} = \frac{x - x_c}{\delta(\epsilon)}, \tag{7}$$

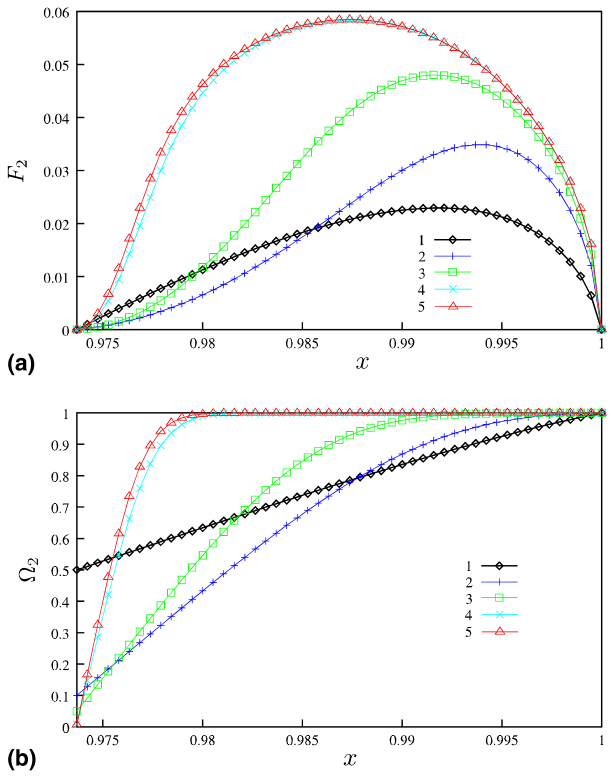

Fig. 5. Evolution of problem $(\mathscr{P}_2)$ solutions as a function of the parameter $\mathscr{R}_{e_2}$. Numerical solutions obtained for $q_1 = 0.7$, $\mathscr{R}_{e_1} = 8$, $x_c = 0.974$ $(q_2/\chi^2 = -6.25)$ and $\mathscr{R}_{e_2} = 16$ (1), 80 (2), 160 (3), 1000 (4), 1231 (5): (a) function F_2; (b) function Ω_2.

where $\delta = \epsilon^{2/3}$ is the thickness of the angular boundary layer. Then, we search the first order of the inner solution as follows:

$$\begin{aligned} F_2(x,\epsilon) &= \alpha_0(\epsilon) f_0(\tilde{x}) + o(\alpha_0), \\ \Omega_2(x,\epsilon) &= \beta_0(\epsilon)\omega_0(\tilde{x}) + o(\beta_0) \end{aligned} \tag{8}$$

and we determine, with the help of the matching conditions, the unknown coefficients: $\alpha_0 = \epsilon^{1/3}$ and $\beta_0 = 1$. Finally, the inner solution can be entirely formulated according to the function g, solution of Ricatti's equation

$$\begin{cases} g'(y) + \dfrac{1}{2} g^2(y) = y, \quad \forall y \in [0, +\infty[, \\ g(0) = 0. \end{cases} \tag{9}$$

Therefore, the inner solutions are

$$\begin{cases} f_0(\tilde{x}) = \left[\dfrac{1 - x_c}{2}\right]^{1/3} g\left(\lambda^{1/3}\tilde{x}\right), \\ \omega_0(\tilde{x}) = \dfrac{1}{\gamma} \displaystyle\int_0^{\lambda^{1/3}\tilde{x}} \exp\left(-\int_0^s g(t)\,\mathrm{d}t\right) \mathrm{d}s, \end{cases} \tag{10}$$

where

$$\lambda = \left[2(1 - x_c)^2 (1 + x_c)^3\right]^{-1} \quad \text{and} \quad \gamma = \int_0^\infty \exp\left(-\int_0^s g(t)\,\mathrm{d}t\right) \mathrm{d}s. \tag{11}$$

One can now observe that the initial condition $g(0) = 0$ of problem (9) leads to $g'(0) = 0$. Then, the first order inner expansions (10) asymptotically satisfy adherence conditions on the cone. This is in agreement with the stresses gap presented in Section 2.2: at this asymptotic approximation, the flow outside the cone does not seem to move in comparison with the flow inside the cone. It's the reason why, at the cone frontier, we obtain the adherence condition in the same way that one must write the adherence condition on a solid boundary.

So, for this asymptotic case, the discontinuity of the stresses is motivated, on the first hand to take into account contact forces from the particles moving inside the fluid, and, on the other hand, to describe the particular behavior of the cone frontier which separates two flows, with one of them which is almost not moving relatively to the second one.

Moreover, the outer and inner expansions enable us to build the composite expansions $F_c^{(2)}$, $\Omega_c^{(2)}$ associated with the functions F_2 and Ω_2. We compute $G_c^{(2)}$ as the composite expansion of the derivative F_2' which gives the radial component u of the velocity field (1). Thus, we obtain the following formulas, for all x in the interval $[x_c, 1[$:

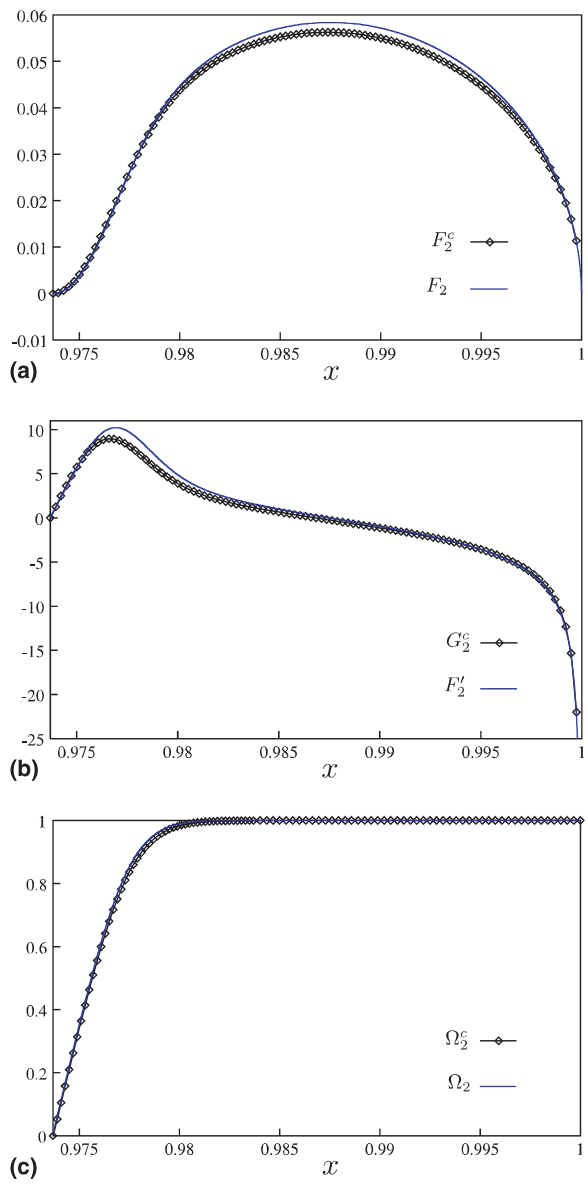

Fig. 6. Validation of composite developments in case ($q_1 = 0.7$, $\mathscr{R}_{e_1} = 8$) and ($q_2 = -4 \times 10^{-4}$, $\mathscr{R}_{e_2} = 10^3$), corresponding to $x_c = 0.974$: (a) function F_2; (b) function F_2'; (c) function Ω_2.

$$
\begin{aligned}
G_2^{\mathrm{c}}(x,\epsilon) &= \epsilon^{-1/3}\left[\frac{\lambda}{2\sqrt{(1-x_{\mathrm{c}})}}\right]^{1/3}\frac{1+x_{\mathrm{c}}-2x}{\sqrt{1-x}}g'\Big([\lambda/\epsilon^2]^{1/3}(x-x_{\mathrm{c}})\Big),\\
F_2^{\mathrm{c}}(x,\epsilon) &= \epsilon^{1/3}\left[\frac{1}{2\sqrt{(1-x_{\mathrm{c}})}}\right]^{1/3}\sqrt{1-x}g\Big([\lambda/\epsilon^2]^{1/3}(x-x_{\mathrm{c}})\Big),\\
\Omega_2^{\mathrm{c}}(x,\epsilon) &= \frac{1}{\gamma}\int_0^{[\lambda/\epsilon^2]^{1/3}(x-x_{\mathrm{c}})}\exp\left(-\int_0^s g(t)\,\mathrm{d}t\right)\mathrm{d}s.
\end{aligned}
\tag{12}
$$

In order to validate these expressions, we compare the formulas (12) with numerical solutions in a given case (see Fig. 6).

Moreover, we are now in position to evaluate the gap of the tangential stresses on the cone frontier. Using formulas (4), on the first hand, and the expressions (6)–(11) on the other hand, when the conditions of the flows—inside and outside the cone—are such that the above asymptotic analysis is valid, one can show that

$$\tau^i_{R_{\mathrm{c}}} = \mathcal{O}(\epsilon^{-2}) \quad \text{and} \quad \tau^i_{\theta_{\mathrm{c}}} = \mathcal{O}(\epsilon^{-2}). \tag{13}$$

This proves that tangential stresses are discontinuous on the cone frontier, at least, when the flow inside the cone swirls very rapidly in comparison with the flow outside the cone.

Finally, using the normalized and complete solution of problem ($\mathscr{P}$)—i.e., the functions defined by $(\chi F_1, \chi\Omega_1)$ on $[0, x_{\mathrm{c}}[$ and (F_2, Ω_2) on $[x_{\mathrm{c}}, 1]$—we are now able to apply them to physical variables to understand the whole characteristics of the fluid motion we modelled.

4. Physical interpretation

The way we choose to model a two cells swirling flow within a separate fictive cone between the cells, allows us to describe a realistic situation, in line with physical observations. To validate this assertion, we present (see Fig. 7) 3D-streamlines built upon the solutions described in the last sections, completed by numerical estimations of the velocity field.

As mentioned in former sections, solutions of problem ($\mathscr{P}$) are satisfying the adherence condition on the ground. They also describe, outside the cone frontier, a flow which is relatively slow in comparison with the one inside the cone. This last flow behaves as a vortical inviscid flow near the axis of the vortex, which is swirling very rapidly.

In a way, these features describe a mature phase of a tornado. Indeed, our model enabled us to evaluate the amplitude of the velocity field, in line with real tornadoes observations. Moreover, our modelling process does

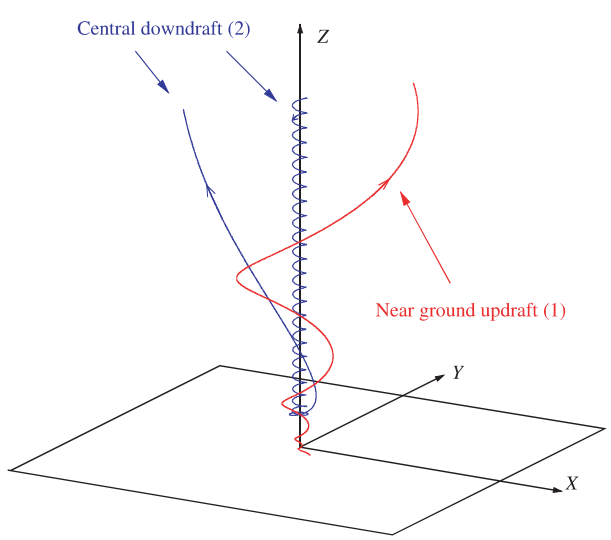

Fig. 7. 3D-streamlines of the fluid motion built on solutions presented in Fig. 6.

include surface forces—along the cone separation between the two cells of the flows—which are translating the integral of dragging forces acting from dust debris of matter inside the fluid. To this end, we set that tangential stresses must absolutely be discontinuous.

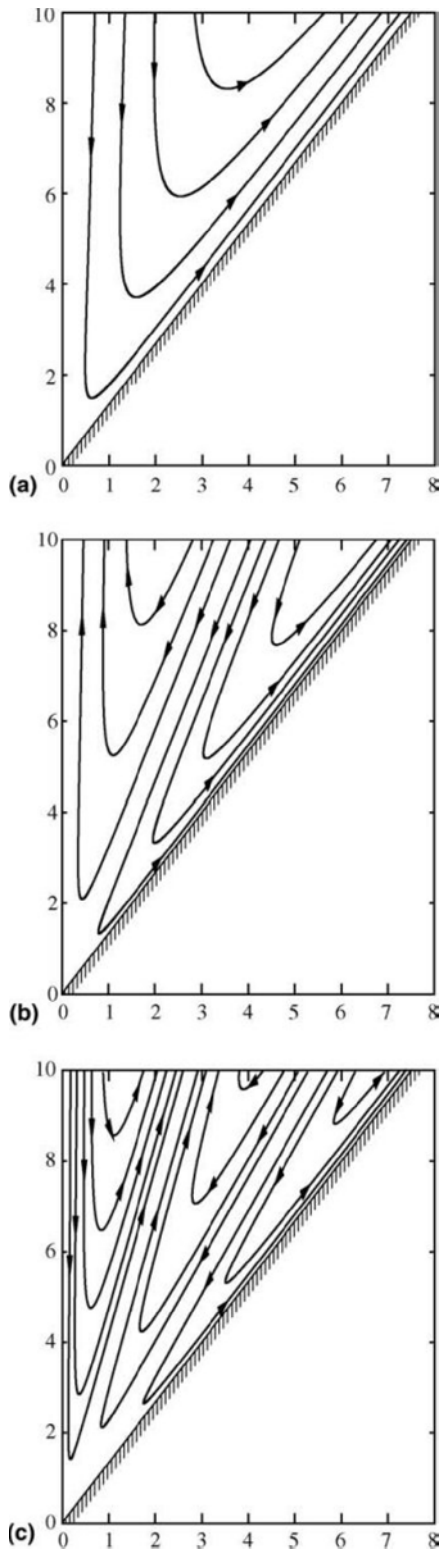

Fig. 8. Kind of fluid motions noticeable with a slip condition on the cone. Streamlines inside the cone are presented in a meridian plane: (a) one cell; (b) two cells; (c) three cells.

In order to evaluate velocity scale resulting from our model, we notice that if the flow outside the cone can be considered laminar, we must change this characteristic inside the cone, because the level of the velocity we do want to describe is too high. Therefore, it is reasonable to consider a turbulent flow inside the cone. Consequently, we introduce the turbulent viscosity ν_t in the definition of the Reynolds number $\mathscr{R}_{e_2}$ characteristic of the flow in cell 2.

To our knowledge, most existing numerical simulations [12], consider this turbulent viscosity approximately equals to 10 $m^2 s^{-1}$. Then, for a Reynolds number $\mathscr{R}_{e_2}$ to equal 1000, the circulation Γ_2 is around 10^4 $m^2 s^{-1}$, which corresponds to the values of the strongest known tornadoes. Then, if we observe the characteristics of a tornado at 100 m of the central axis and high enough in the storm, we find that the value of the azimuthal velocity is about 10^2 m s^{-1}. This proves that the values of our model are in line with those observed in real tornadoes.

This numerical result is directly linked to our modelling process, in relation with the discontinuity of tangential stresses on the cone frontier. Indeed, because of this extra degree of freedom we were in position to increase without limit the value of the Reynolds number $\mathscr{R}_{e_2}$ to achieve realistic values of the velocity, observed in tornadoes.

The final point we would like to make is directly linked to our modelling of the two rotating cells, inside and outside a given cone. In fact, we have considered independent families of conical flows which are slipping on a given cone surface. Concerning the possible flows which are available inside the cone, we have found new possibilities of flows, regarding Serrin's model.

Because we considered a slip condition on the cone frontier mentioned above, we outlined a flow composed by three cells inside the cone (see Fig. 8(c)). This situation does not exist when an adherence condition on a given wall is being considered.

The main features of these three cells are: near the central axis of the swirling vortex, the flow is descending as a downdraft. In the neighborhood of the cone surface—where the fluid is sliding—the flow is directed outward.

Then, two specific and intermediate directions emerge and produce two jets. So, three local and continuous flows exist inside the cone, in such a manner that the outflow along the cone, we mentioned above, is not the continuity of the descending flow near the central axis—as in the case (a) of Fig. 8.

We have paid great attention to this kind of new flows, because atmospherical tornadoes often develop several jets noticeable by the dust ejected from the core of the tornado [3].

Consequently, a three cells rotating downdraft may participate in describing this above situation.

References

[1] J. Chaskalovic, Sur la modélisation mathématique des tornades atmosphériques: Genèse et dégénérescence, Thèse de l'Université Pierre et Marie Curie, 30th January, 1991.
[2] J. Serrin, The swirling vortex, Phil. Trans. Roy. Soc. Lond. A 271 (1972) 320–360.
[3] J. Serrin, The swirling vortex, Phil. Trans. Roy. Soc. Lond. A 271 (1972) 357–358.
[4] M. Goldshtik, V. Shtern, Collapse in conical viscous flows, J. Fluid Mech. 218 (1990) 483–508.
[5] E. Kessler, Thunderstorm Morphology and Dynamics, University of Oklahoma Press, Norman and London, 1985.
[6] R.L. Gall, Internal dynamics of tornado-like vortices, J. Atmos. Sci. 39 (12) (1982) 2721–2736.
[7] D.S. Nolan, A.S. Almgren, J.B. Bell, High Reynolds number simulations of axisymmetric tornado-like vortices with adaptive mesh refinement, in: Conference on European Tornadoes and Severe Storms, Toulouse, 1–4 February, 2000.
[8] A. Chauvière, Contributions à la modélisation d'une ligne semi-infinie tourbillonnaire: Applications aux tornades atmosphériques, Thèse de l'Université Pierre et Marie Curie, 17th December, 2001.
[9] V. Shtern, F. Hussain, Hysteresis in swirling jets, J. Fluid Mech. 309 (1996) 1–44.
[10] R. Fernandez-Feria, J. Fernandez de la Mora, M. Perez-Saborid, A. Barrero, Conically similar swirling flows at high Reynolds numbers, Quart. J. Mech. Appl. Math. 52 (Part 1) (1999) 1–53.
[11] V. Shtern, F. Hussain, Collapse, symmetry breaking, and hysteresis in swirling flows, Annu. Rev. Fluid Mech. 31 (1999) 537–566.
[12] D.S. Nolan, B.F. Farrell, The structure and dynamics of tornado-like vortices, J. Atmos. Sci. 56 (16) (1999) 2908–2936.
[13] J.M. Burgers, A mathematical model illustrating the theory of turbulence, Advan. Appl. Mech. 1 (1948) 197–199.
[14] N. Rott, On the viscous core of a line vortex, Z. Angew. Math. Phys. 96 (1958) 543–553.